Injection of solar near-relativistic electrons associated with radio bursts

Neus Agueda*, **Rami Vainio***, **David Lario**†, **Blai Sanahuja**‡ **and Laurianne Palin***

**Department of Physics, University of Helsinki, 00014 Helsinki, Finland*
†*Applied Physics Laboratory, The Johns Hopkins University, Laurel, MD 20723-6099, USA*
‡*Departament d'Astronomia i Meteorologia, Universitat de Barcelona, 08028 Barcelona, Spain*

Abstract. Solar near-relativistic (NR) electrons are observed in near-Earth space following different types of solar transient activity, such as solar flares and coronal mass ejections (CMEs). We have developed an inversion method that allows us to infer both the solar injection profile and the interplanetary transport conditions of NR electrons by fitting the directional intensities observed by the *ACE* spacecraft at 1 AU. We apply the inversion method to six large NR electron events temporally associated with type III and type II radio bursts. For four events, the source injecting particles is active for a long period of time (> 3 h) whereas in two events, the injection profile shows several short (< 15 min) injection episodes. We compare the inferred injection profiles with 20 kHz to 14 MHz radio observations by WAVES instrument on the *Wind* spacecraft. Strong type II radio bursts, revealing shock waves in the corona, are associated with long-lasting injection profiles, which suggests that coronal shocks have an important role in the production of at least some heliospheric NR electron events. On the other hand, for other events, short injection episodes are in temporal correlation with type III radio bursts. In such cases, NR electrons are more likely injected due to processes of coronal restructuring (magnetic reconnection) following the CME lift-off.

Keywords: Sun: particle emission – Sun: radio radiation – Sun: flares – Sun: coronal mass ejections

I. INTRODUCTION

Solar near-relativistic (NR) electrons (> 30 keV) are usually observed in interplanetary space as discrete events following different types of solar transient activity [1], such as flares and coronal mass ejections (CMEs). In situ observations of NR electron events in the heliosphere can be used to infer the mechanisms of electron production at the Sun (e.g., [2], for a review).

Comparisons between the timing of solar transient electromagnetic phenomena and the inferred starting time of the electron injection have been used to examine the solar sources of NR electrons. Observational studies have suggested that most NR electron events result from flares [2]. But other mechanisms, such as magnetic restructuring in the aftermath of CMEs [3], [4]

or acceleration at shocks driven by fast (> 1000 km s^{-1}) CMEs [5], [6] have also been proposed as a mechanism for the production of NR electrons.

Solar radio bursts provide diagnostics of the electron acceleration mechanisms. Type III radio bursts drift rapidly to low frequencies, and often occur in groups lasting several minutes at ∼14 MHz. They are usually taken as signatures of the flare impulsive phase [7] and trace 2–100 keV electron streams as they propagate along open field lines from flaring regions near the Sun into the interplanetary medium [8]. Type II bursts are distinguished by their slower drift rates and longer lasting emission relative to type III bursts and are attributed to shocks moving out in the solar corona with speeds of ∼1000 km s^{-1} [7].

The shock acceleration hypothesis was tested by studying the association of NR electron events with type II radio bursts and CMEs [9]. The event associations with type II bursts were found to be 37%/17% for metric/decametric-hectometric (DH) type II bursts and only ∼ 50% of the electron events were associated with wide (> 60°) and fast (> 900 km s^{-1}) CMEs. The poor association led to the conclusion that at least some, and perhaps most, NR electron events do not originate from coronal shocks [9]. In a later study, Kahler et al. [6] found that those NR electron events showing highly anisotropic pitch-angle distributions at 1 AU for long (> 2 h) time periods are well associated with metric and DH type II bursts, supporting the possibility of a class of shock-accelerated NR electron events.

Recent work based on fitting NR electron intensities observed at 1 AU allows us to compare solar NR electron injection profiles with corresponding white-light, X-ray and radio signatures [10]. Inferring the injection profile is a powerful tool to distinguish between different mechanisms of particle acceleration and release into interplanetary space.

In this paper, we address the question of the relative contributions that flare and shock acceleration processes have in large NR electron events. We make use of simulations of the propagation of NR electrons along the interplanetary magnetic field under reasonable fiducial conditions to fit the directional intensities observed at 1 AU by the LEFS60 telescope of the EPAM experiment on board the *Advanced Composition Explorer* (*ACE*) [12] and thus infer the electron injection profile close

to the Sun and the interplanetary transport conditions. We compare the inferred injection profiles with the low-frequency (~14 MHz) type III and DH type II bursts observed by the WAVES instrument [11] on board the *Wind* spacecraft.

In Section 2, we present the characteristics of the NR electron events selected for the study and the associated radio emissions. We review the transport model and the fitting technique in Section 3. Section 4 gives an overview of the results of deconvolving the directional intensities observed during the selected events. Results are summarized in Section 5.

II. DATA ANALYSIS

A. Event selection

We analyze 72 s averages of the electron intensities measured by the LEFS60 telescope of the EPAM experiment on board *ACE* [12] in three energy ranges: E'2 (62–102 keV), E'3 (102–175 keV) and E'4 (175–312 keV). The LEFS60 detector is pointed 60° from the spacecraft spin axis. As the spacecraft spins, the solid angle swept by the detector is divided into eight sectors, each 45°, providing directional information of the incoming particles. We also make use of magnetic field and solar wind data provided by the MAG [13] and SWEPAM [14] instruments on board *ACE* to characterize the interplanetary magnetic field (IMF) during the events.

We identified the NR electron events observed by the LEFS60 telescope between 2000 and 2007 meeting the following three criteria:

- Significant enhancement of NR electron intensities, i.e., spin-averaged peak intensities at least 30 times higher than the pre-event background intensities in the E'4 energy channel
- Negligible proton contamination in the electron energy channels of the LEFS60 telescope
- Quietness in the interplanetary medium, with stable IMF and steady solar wind parameters from one hour prior to the onset of the event until six hours later.

We found 15 NR electron events that fulfill these three criteria. Two electron events were excluded from the list because there is evidence of previous events that caused high background levels. By looking for the onset time of the events at intensity levels which are a fixed percentage of the maximum intensity in each energy channel [15] and requiring velocity dispersion at their onset, we found that seven other events had to be excluded. Therefore, 6 of 15 events were selected for further analysis.

For the selected events, we checked that the pitch-angle distributions observed by the LEFS60 telescope covered a wide range in pitch-angle cosine. We found a reasonably good coverage in pitch-angle cosine ($\geq 70\%$) that qualified them to be studied (see [16] for a detailed analysis of the pitch-angle coverage by the LEFS60 telescope).

Columns (1)–(5) of Table I give information about the selected NR electron events: date; time of the onset, t_0 and rise time (i.e. the time interval between the onset and the maximum intensity) in the E'4 energy channel; time interval selected for simulation; and event strength, S, defined as the logarithm of the ratio between the spin-averaged peak intensity, I_p, and the spin-averaged mean intensity of the pre-event background, I_b, in the E'4 energy channel; thus $S = \log_{10}(I_p/I_b)$.

The selected events show, as a whole, a median event strength of 2.5 and rise times longer than ~1 h. The period of modelization has been chosen to be ~3–4 h, since we aim at characterizing the solar injection profile of the first arriving electrons at 1 AU.

B. Radio data

All the selected events were preceded by fast-drift radio bursts. We use 20 kHz–14 MHz radio spectrograms acquired by the WAVES experiment on the *Wind* spacecraft [11] and available on the WAVES Web site[1]. The spectral plots allowed us to estimate the start and end times of the associated type III radio bursts at 14 MHz, to the nearest 5 minutes. These times are given in column (6) of Table I. All type III radio bursts happened in association with the observations of soft X-ray emission from the Sun and Hα brightenings from the western hemisphere of the Sun[2]; except for the 2004 Sep 19 event when no Hα brightening was observed.

We obtained the start/end times and the characteristics of the DH type II radio emission from the WAVES Web site list[1]. Columns (7)–(8) of Table I give the times of the type II radio bursts and the qualitative assessments of the emission provided on the WAVES Web site. Three out of the six of the selected electron events were associated with strong type II bursts. The other three events were associated with diffuse, sporadic and intermittent type II radio bursts. CMEs with speeds >1000 km s^{-1} were observed in association with most of the electron events[3]; the speeds of the CMEs observed in association with the 2004 Sep 19 and the 2005 Jun 16 electron events were not measured due to lack of observations.

III. TRANSPORT AND INJECTION MODELING

We fit sectored intensities observed by the LEFS60 telescope of the EPAM experiment on *ACE* by simulating the interplanetary transport of NR electrons and then determining the optimal injection function near the Sun.

A. Interplanetary transport

We use a Monte Carlo model to simulate the interplanetary transport of SEPs injected at the root of an Archimedean spiral magnetic field line. The transport processes included are the following: particle streaming along the magnetic field lines, pitch-angle focusing by

TABLE I: Solar NR Electron Events and Associated Radio Bursts

	NR Electron events				Radio emission				Injection type[c]
Date	t_0	Rise	Period	S	Type III[a]	Type II[b]			
	(UT)	(min)	(UT)		(UT)	(UT)	Comments		(UT)
(1)	(2)	(3)	(4)	(5)	(6)	(7)	(8)		(9)
2000 Nov 08	22:55	60	22:55–03:00	4.3	22:55-23:05	23:20-12:00*	Intense		L
2001 Dec 26	05:25	84	05:20–09:00	2.9	05:15-05:20	05:20-05:00*	Strong F-H		L
2002 Aug 24	01:20	56	01:20–04:20	1.8	01:05-01:15	01:45-03:25	Strong F, Weak H		L
2002 Dec 19	21:55	45	21:50–02:00	2.3	21:40-21:55	21:45-22:30	Broad, diffuse band		S
2004 Sep 19	17:25	85	17:10–20:45	2.2	16:55-17:30	17:15-18:15	Very sporadic		L
2005 Jun 16	20:25	130	20:25–24:00	1.7	20:10-20:20	20:25-21:40	Very intermittent		S

[a] Duration of the type III bursts estimated at ∼14 MHz to the nearest 5 min.
[b] DH type II bursts reported in the WAVES Web site. Times with * refer to the next following day. (F = fundamental; H = harmonic).
[c] Electron injection type inferred from fitting the directional electron intensities observed by *ACE* at 1 AU (S = short; L = long-duration).

the diverging IMF, pitch-angle scattering by magnetic fluctuations, adiabatic deceleration resulting from the interplay of scattering and focusing and solar wind convection [17], [18]. The results of the simulation give the directional distribution of particles at 1 AU, as a function of time and energy range of interest (see [10] for details).

As initial condition we consider all particles to be injected instantaneously at two solar radii from the center of the Sun. Thus, the results of the simulation are expressed in terms of Green's functions of particle transport. The energy spectrum of the solar source is described by a power law ($dN/dE \propto E^{-\gamma_s}$) with spectral index γ_s, which is estimated from the observational data (see [10]).

In the solar wind frame, the pitch-angle diffusion coefficient can be expressed as $D_{\mu\mu} = \nu(1 - \mu^2)/2$, where ν is the scattering frequency and μ is the particle pitch-angle cosine. We assume $\nu(\mu) = \nu_0 \left(\frac{|\mu|}{1+|\mu|} + \epsilon \right)$, where ϵ allows us to simulate different scattering conditions, from quasi-isotropic ($\epsilon \geq 1$) to fully anisotropic ($\epsilon = 0$, totally decoupled hemispheres in the μ-space). The scattering rate, ν_0, is determined from the mean free path parallel to the field $\lambda_{||}$, or the radial mean free path λ_r, which are related by

$$\frac{\lambda_r}{\cos^2 \psi} = \lambda_{||} = \frac{3v}{4} \int_{-1}^{+1} \frac{1 - \mu^2}{\nu(\mu)} d\mu \qquad (1)$$

where v is the particle speed and ψ is the angle between the magnetic field and the radial direction [19]. Particle transport perpendicular to the magnetic field is neglected. Following the procedure adopted in previous works, we assume the radial mean free path to be constant, independent of the radial distance and energy [20], [21].

B. Fitting sectored intensities

The goal is to solve the inversion problem of inferring the transport parameters (i.e. λ_r, ϵ) and the injection time profile at the Sun from a set of in-situ measured sectored intensities $I^s(t)$, where $I^s(t)$ is the intensity measured at time t by sector s in a given energy channel. By taking into account the angular response of the sectors scanned by the LEFS60 telescope, we are able

to transform the simulated pitch-angle distributions into sectored intensities measured by the telescope [10]. The modeled sectored intensities, $M^s(t; \lambda_r)$, in sector s can be written as

$$M^s(t; \lambda_r) = \int_{T_1}^{T_2} dt' g^s(t, t'; \lambda_r) q(t'), \qquad (2)$$

where $q(t)$ -to be determined- represents the electron injection function and $g^s(t, t'; \lambda_r)$ represents the contribution of an impulsive injection to the modeled intensities for a given sector s, at a given time t, when the injection of NR electrons took place at time t'.

Taking into account the eight sectors of the telescope and discrete values of time, the best-fit injection function can be determined by comparing the modeled intensities with the observations. Let b be the sector-averaged background intensity and $J_i = I_i - b$, where $i = 1, 2, ..., n$ numbers the observational points. We want to derive the m-vector $\vec{q}$ that minimizes the length of the n-vector $\vec{J} - \vec{M}$, that means minimizing the value of $||\vec{J} - \vec{M}|| \equiv ||\vec{J} - \mathbf{g} \cdot \vec{q}||$, subject to the constraint that $q_j \geq 0 \; \forall j = 1, 2, ..., m$, where j numbers the injection times. The best-fit injection function corresponds to a combination of m delta-function injection amplitudes at times t_j. To solve this inversion problem and obtain the best-fit injection values, we use the non-negative least squares method [22].

The best-fit transport parameters (λ_r and scattering case) are determined by minimizing a goodness-of-fit estimator which computes the sum of the squared logarithmic differences between the observational and the modeled data in each energy channel. The calculation of the goodness of the fit is restricted to the time interval selected. The goodness-of-fit estimator of the whole fit is obtained by adding the values obtained for each energy channel.

IV. RESULTS

We simulate the selected NR electron events following the same procedure as described in [10]. We consider three scattering cases: isotropic scattering ($\nu(\mu) = \nu_0$) and two μ-dependent scattering cases, one with $\epsilon = 0.10$ and one with $\epsilon = 0.01$, for several values of λ_r, quasi-logarithmically spaced between 0.04 AU and 1.5 AU.
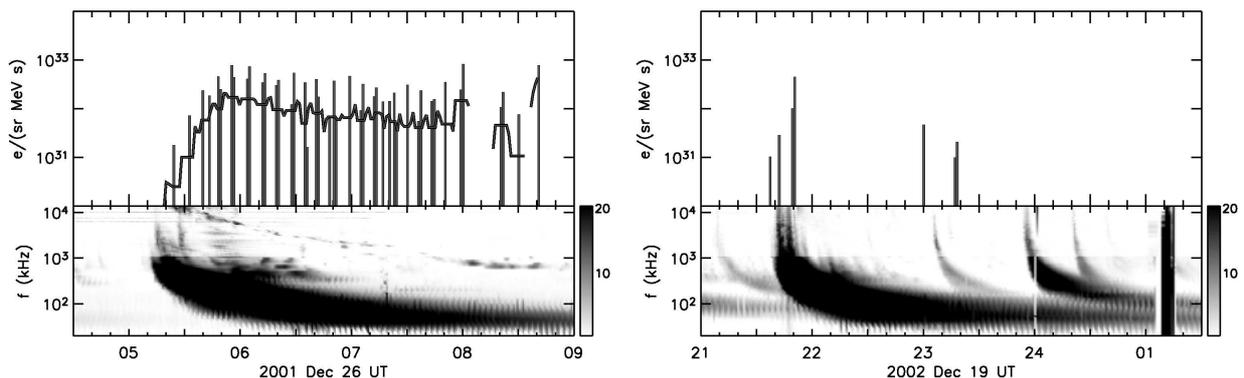
Fig. 1: Electron injection profiles derived for the E'2 energy channel (injection times are shifted by 8 min to account for the light travel time). In addition to the fit result (histogram), a smoothed curve obtained by six-point moving average is shown in the left panel. Radio flux (in dB over background) observed by *Wind*/WAVES.

The fits succeed in reproducing most of the features of the intensities observed in the eight different sectors in the E'2, E'3 and E'4 energy channels. All the selected events are best fitted assuming $\lambda_r \leq 0.24$ AU (Note that other events require larger λ_r such as the event analyzed in [10]). According to the values of the goodness of fit estimator, three of the events studied here can be best fitted assuming μ-dependent scattering and three events assuming isotropic pitch-angle scattering.

The inferred injection profile of four of the events displays a prolonged injection lasting at least three hours, whereas for two of the events the injection profile is composed by several sparse short (< 15 min) injection episodes. Column (9) of Table I lists the type of injection profile that best fits the selected events. The injection profile inferred for the 2001 Dec 26 and the 2002 Dec 19 events in the E'2 energy range is shown in Figure 1 to illustrate the two categories, respectively. The injection profile appears patchy in both cases, however, if we convolve the modeled Green's functions by a smoothed injection profile (see smoothed curve in Figure 1) in the case of a prolonged injection, the fit does not practically differ from the best fit.

Four NR electron events associated with strong type II radio bursts, revealing shock waves in the corona, show long-lasting injection profiles, which suggests that, in these cases, coronal shocks are most likely the source of the NR electrons observed in the heliosphere. On the other hand, the injection of two NR electron events shows sparse short injection episodes while intermittent and broad type II radio bursts are observed. Their sparse occurrence, well correlated with several type III radio bursts, suggests that they could be related to processes of coronal restructuring (magnetic reconnection) occurring after the CME lift-off.

V. CONCLUSIONS

Directional particle intensities observed at 1 AU allow us to infer the injection profile of NR electrons at the Sun by simulating the propagation of solar energetic particles along the IMF. The injection profile allows us to gain insight on the solar sources of these electrons as it provides key information about the injection timing and duration.

We simulated six large NR electron events and found that coronal shocks and reconnection processes both seem to play a role in the injection of NR electrons. The observation of *strong* type II bursts may be a good guide to infer shock acceleration of NR electrons since coronal shocks producing strong type II radio bursts are associated with long-lasting (> 3 h) injection profiles.

REFERENCES

[1] R.P. Lin, Solar Phys., 12, 266, 1970.
[2] S.W. Kahler, Space Science Rev., 129, 359, 2007.
[3] D.J.F. Maia, and M. Pick, Astrophys. J., 609, 1082, 2004.
[4] K.L. Klein, S. Krucker, G. Trottet, and S. Hoang, A&A, 431, 1047, 2005.
[5] G.M. Simnett, E.C. Roelof, and D.K. Haggerty, Astrophys. J., 579, 854, 2002.
[6] S.W. Kahler, H. Aurass, G. Mann, and A. Klassen, Astrophys. J., 656, 567, 2007.
[7] J.P. Wild, S.F. Smerd, and A.A. Weiss, Annu. Rev. Astron. Astrophys., 1, 291, 1963.
[8] R.P. Lin, Solar Phys., 100, 537, 1985.
[9] S.W. Kahler, H. Aurass, G. Mann, and A. Klassen, Proc. IAU Symposium no. 226, 338, 2005.
[10] N. Agueda, R. Vainio, D. Lario, and B. Sanahuja, Astrophys. J., 675, 1601, 2008.
[11] J.L. Bougeret et al., Space Science Rev., 71, 5, 1995.
[12] R.E. Gold et al., Space Science Rev., 86, 541, 1998.
[13] C.W. Smith et al., Space Science Rev., 86, 613, 1998.
[14] D.J. McComas et al., Space Science Rev., 86, 563, 1998.
[15] J. Lintunen, and R. Vainio, A&A, 420, 343, 2004.
[16] N. Agueda, R. Vainio, D. Lario, and B. Sanahuja, Adv. Space Res., *submitted*, 2009.
[17] L. Kocharov, R. Vainio, G.A. Kovaltsov, and J. Torsti, Solar Phys., 182, 195, 1998.
[18] R. Vainio, L. Kocharov, and T. Laitinen, Astrophys. J., 528, 1015, 2000.
[19] K. Hasselmann, and G. Wibberenz, Z. Geophys., 34, 3533, 1968.
[20] M.B. Kallenrode, G. Wibberenz, and S. Hucke, Astrophys. J., 394, 351, 1992.
[21] W. Dröge, Astrophys. J., 589, 1027, 2003.
[22] C.L. Lawson, and R.J. Hanson, Solving Least Squares Problems (Englewood Cliffs: Prentice-Hall), 1974.